Annals of Biomedical Engineering:

Investigating the longitudinal effect of ovariectomy on bone properties using a novel spatiotemporal approach

Yongtao Lu[1,2], Yue Liu[3], Chengwei Wu[1,2,*] and Junyan Li[4*]

[1]State Key Laboratory of Structural Analysis for Industrial Equipment, Dalian University of Technology, Dalian, China

[2]Department of Engineering Mechanics, Dalian University of Technology, Dalian, China

[3] Department of Mechanical Engineering, National University of Singapore, Singapore

[4] Department of Design Engineering and Mathematics, School of Science and Technology, Middlesex University, London, UK

Running head: Longitudinal Effect of Ovariectomy on Bone Properties

CORRESPONDING AUTHORS:

1. Junyan Li, PhD

Department of Design Engineering and Mathematics, School of Science and Technology, Middlesex University, London, UK
Phone: +44 02084115403
Email: j.y.Li@mdx.ac.uk

2. Chengwei Wu, PhD

Vice Dean of FVEM
Department of Engineering Mechanics, Dalian University of Technology, No. 2 Linggong Road, 116024, Dalian, China
Phone: +86 (0)411 84706353
Email: cwwu@dlut.edu.cn

Word count (including references):6205

Number of tables: 2

Number of figures: 7

Abstract (200 words)

Osteoporosis is the most common bone disease. However, the mechanism of osteoporosis-induced alterations in bone is still unclear. The aim of this study was to investigate the effects of osteoporosis on the structural, densitometric and mechanical properties of the whole tibia using *in vivo* μCT imaging, spatiotemporal analysis and finite element modeling. Twelve C57Bl/6 female mice were adopted. At 14 weeks of age, half of the mice were ovariectomized (OVX), and the other half were SHAM-operated. The whole right tibia was scanned using an *in vivo* μCT imaging system at 14, 16, 17, 18, 19, 20, 21 and 22 weeks. The image datasets were registered in order to precisely quantify the bone properties. The results showed that OVX led to a significant increase in the endosteal area across the whole tibia four weeks after OVX intervention but did not have a significant influence on the periosteal area. Additionally, the bone volume and mineral content significantly decreased only in the proximal regions, but these decreases did not have a significant influence on the stiffness and failure load of the tibia. This study demonstrated the application of a novel spatiotemporal approach in the comprehensive analysis of bone adaptations in the spatiotemporal space.

Keywords: Osteoporosis, mouse tibia, *in vivo* μCT, spatiotemporal analysis, finite element modeling

1. Introduction

Osteoporotic fracture is one of the major health problems affecting the aging population.[1] Using human subjects to study osteoporosis is challenging because the changes within human bone structures span a prolonged period (over years) and vary substantially among individuals. The progression of osteoporosis in humans can be efficiently simulated by conducting an ovariectomy (OVX) in rodents, and this has become a well-established approach for investigating the mechanism of osteoporosis.[2-4] However, most of the previous studies are based on cross-sectional analyses (i.e., sacrifice the animals at each time point of investigation) and only provide results from a portion of the whole bone (e.g., the proximal region of the mouse tibia or midshaft).[2-6] These studies lack information on following adaptations of the same bone over the whole bone space.

To address these issues, there is a need to develop spatiotemporal models across the whole bone space, which can be realized by combining *in vivo* micro-computed tomography (μCT) imaging and image registration. *In vivo* μCT imaging is non-invasive and enables changes in the same bone to be monitored longitudinally.[7-9] Moreover, the measurement variability caused by the inter-subject differences within a study cohort can be substantially reduced using *in vivo* longitudinal imaging because each subject can serve as its own control using image registration.[10] Recently, *in vivo* μCT imaging has been used to study the effects of medical intervention and mechanical loading on the morphometric and densitometric properties of mouse bone.[8-12] However, only a portion of the bone (e.g., the proximal region of the tibia or tibial midshaft) was used as the region of interest in these studies. The longitudinal effect of OVX on the structural and densitometric properties of the whole tibia, which has commonly been used to study clinical bone fractures, is

unknown. This knowledge could provide additional important information on the mechanism of osteoporosis-induced bone changes in animal models. Furthermore, structural changes in areas such as the endosteal and periosteal bone areas in the spatiotemporal space could comprehensively unveil the mechanism of bone adaptation during osteoporosis.

Additionally, micro-finite element (μFE) models reconstructed from μCT images can be used to non-invasively investigate the longitudinal effect of medical intervention on the mechanical behavior of the same bone. *In vivo* μCT image-based μFE models have been used to investigate the effect of medical intervention on the mechanical behavior of bone[11] and the mechanism of bone mechano-regulation.[13-16] However, no previous studies have monitored the longitudinal effect of OVX on the mechanical behavior of bone across the whole tibia, and little is known about the relationship between the mechanical behavior of bone and the spatiotemporal changes in bone structural and densitometric properties. This knowledge could provide important information on the effect of changes (e.g., induced by OVX intervention) in bone structural and densitometric properties on the fracture resistance capability of the bone and thus could unveil the in-depth mechanism of osteoporosis.

The aim of this study is to investigate the longitudinal effect of OVX on the structural, densitometric and mechanical properties of bone across the whole mouse tibia using a novel methodology combining *in vivo* μCT imaging, spatiotemporal analysis and finite element modeling.

2. Materials and Methods

2.1 *In vivo* μCT imaging

Twelve female C57Bl/6 mice were used in this study. They were divided into OVX (N = 6) and SHAM (N = 6) (control) groups and received surgery at 14 weeks of age. The right lower limbs of the mice (including the whole tibia) were imaged at 14, 16, 17, 18, 19, 20, 21 and 22 weeks (eight times) using an *in vivo* μCT system (vivaCT 80, Scanco Medical, Switzerland) with an isotropic image voxel size of 10.4 μm, a voltage of 55 keV, a tube current of 145 μA and an integration time of 200 ms. All of the procedures complied with the UK Animals Act 1986 and were approved by the University of Sheffield Research Ethics Committee.

To evaluate the effect of ionizing radiation on the results, the twelve mice were sacrificed at 24 weeks of age, and then both tibiae were scanned using the same imaging protocol as used for the *in vivo* imaging. The imaging of the left tibia after sacrificing the mouse was to ensure that no radiation was induced on the left tibia. The results calculated from the *ex vivo* images (mice at 24 weeks of age) were compared between the irradiated (right) and non-irradiated (left) contralateral tibiae.

2.2 Image processing

The image datasets were processed based on the spatiotemporal quantification method developed previously (**Fig. 1**).[17] Briefly, one tibia from week 14 was used as the reference. The long (proximal-distal) axis of this tibia was aligned along the z-axis (**Fig. 1b**). The follow-up scans of the same tibia were rigidly registered to the reference tibia using Quasi-Newton optimizer and Euclidean distance as the similarity measure (Amira 5.4.3, FEI Visualisation Sciences Group, France) in a stepwise manner, e.g., the tibia scanned at time point j+1 was registered to the same tibia scanned at time point j (**Fig. 1b-d**). For the tibiae from other mice, first, the week-14 datasets were rigidly registered to the reference tibia, and then follow-up scans of these tibiae were rigidly registered in a stepwise manner (tibia scanned at

time point j+1 were registered to the same tibia scanned at time point j). To evaluate the effect of ionizing radiation on the results, the right tibiae were rigidly registered to the reference tibia using the same setting of image registration. Then, the left tibiae were mirrored and registered to the corresponding right tibiae. Following the registration, the images were transformed to the new positions and resampled using the Lanczos kernel. In the resampled images, the tibial length (L) was measured from the most distal pixel to the most proximal pixel of the mouse tibia. A region of 80% of the tibia starting from the area below the proximal growth plate was selected as the volume of interest (VOI), which was then partitioned into 10 compartments, each with an equal length in the z-direction (**Fig. 1e**).

In each compartment, the structural and densitometric parameters of the mouse tibia, quantified in the present study, included bone mineral content (BMC, units of mg hydroxyapatite (HA)), tissue mineral density (TMD, units of mg HA/cm^3), bone volume (BV, units of mm^3), tibial endosteal area (TEA, units of mm^2) and tibial periosteal area (TPA, units of mm^2). In addition, the cortical and trabecular bones in the most proximal compartment (C01 in **Fig. 1f**) were segmented using a well-developed automatic segmentation approach.[18] BMC, TMD and BV in the cortical part (C01Ct) were quantified. Because there are almost no trabecular bones in the compartments from C02 to C10, no separation of cortical and trabecular parts was performed for other compartments. When calculating these parameters, the grayscale images were first smoothed using a Gaussian filter (convolution kernel [3 3 3], standard deviation = 0.65) in order to reduce the effect of image noise. Then, the HA-equivalent bone mineral density (BMD) value in each image voxel was calculated from the CT grayscale values using the calibration law provided by the manufacturer and checked weekly using a five-rod densitometric calibration phantom. The

grayscale images were binarized using a threshold, which was 25.5% of the maximal grayscale value,[19] and bone masks (regions occupied by bone) were defined using the binary images. Based on the image BMD, the BMC and TMD in each compartment were calculated as the total bone minerals over the masked bone regions and as the mean mineral density within the masked bone regions, respectively. TEA and TPA were calculated as the areas enclosed by the endosteal and periosteal surfaces of mouse tibiae, respectively.[20]

To visualize the longitudinal changes in tibial TEA and TPA in both the OVX and SHAM groups, for the data obtained at week j (j = 16, … , 22), the TEA and TPA in each compartment were presented as the differences between the values in week 14 and week j, normalized with respect to the baseline (week 14) values in the OVX and SHAM groups, respectively. Changes in tibial BV, TMD and BMC in each compartment were represented as the mean relative percentage difference ($\boldsymbol{\delta D\%_j}$) between the OVX and SHAM groups:

$$\boldsymbol{\delta D\%_j} = \left(\Delta \boldsymbol{B_j} - \Delta \boldsymbol{A_j}\right) \Big/ \boldsymbol{REF_j} \times \mathbf{100} \qquad \textbf{(1)}$$

where

$$\Delta \boldsymbol{A_j} = \frac{\sum_{i=1}^{n1}\left(\boldsymbol{BP_{i,j}^{Sham}} - \boldsymbol{BP_{i,14}^{Sham}}\right)}{n1}$$

$$\Delta \boldsymbol{B_j} = \frac{\sum_{i=1}^{n2}\left(\boldsymbol{BP_{i,j}^{Ovx}} - \boldsymbol{BP_{i,14}^{Ovx}}\right)}{n2}$$

$$\boldsymbol{REF_j} = \frac{\sum_{i=1}^{n1} \boldsymbol{BP_{i,j}^{Sham}}}{n1}$$

$n1$ and $n2$ are the numbers of mice in the SHAM and OVX groups, *j* represents the week index (*j* = 16, …, 22), *i* represents the mouse number index, and $\boldsymbol{BP}$ represents the bone parameter of BV, TMD or BMC.

2.3 Measurement errors associated with the image processing pipeline

In order to properly interpret the differences between groups, the measurement errors associated with the image processing pipeline were quantified. To do this, the right tibiae of eight 14-week-old C57Bl/6 female mice were measured four times each in the *in vivo* μCT scanner with repositioning of the tibiae between scans using the same scanning set-up. The repeated scan image datasets were processed by following the procedures presented in a previous reproducibility study.[17] Precision errors (PEs) and intraclass correlation coefficients (ICCs) were calculated to characterize the measurement errors.[17]

2.4 Finite element analysis

FE analysis was performed to evaluate the longitudinal effect of OVX intervention on the mechanical behavior of mouse tibiae. In brief, a connectivity filter was first used to remove all unconnected bone islands in the transformed binary images of tibial VOI, and then homogeneous μFE models of mouse tibiae were generated (**Fig. 1g**) by converting each bone voxel into an 8-node hexahedron element using in-house-developed Matlab code (Matlab 2015a, The Mathworks, Inc. USA). Each tibia was modeled as an isotropic, linear elastic material with a Young's modulus of 14.8 GPa and Poisson's ratio of 0.3.[21-22] The boundary condition applied to the μFE models was chosen to represent the loading condition commonly used in the literature for investigating the mechanical behavior of mouse tibiae,[14,23] e.g., the uniaxial compression. In detail, the nodes in the most proximal four layers of tibial VOI (approximately 0.25% of the tibial length) were constrained in all degrees of freedom, and a displacement of 1.00 mm was applied on the nodes in the most distal four layers of tibial VOI (**Fig. 1g**). The stiffness and failure load of mouse tibiae were calculated from the FE analysis. The stiffness was calculated by dividing the reaction forces (summed up over all the constrained nodes at the proximal site) by the

displacement of 1.00 mm. The failure load of mouse tibiae was calculated using the maximum principal strain criterion, which has been validated *in vitro* [24] and *in vivo* [25] in the continuum FE models. In short, the tibial failure load was determined from the histogram plot of principal strains and was the value when 5% of bone tissues in the region of investigation were over the principal strain limits (7300 με as the tensile strain limit and 10300 με as the compressive strain limit).[24,26] When calculating the failure load, Saint Venant's principle was applied to minimize the influence of the boundary conditions on the results and thus the region of investigation was approximately 2.06 mm (approximately 14.25% of the tibial length) away from the proximal end of the VOI and 1.77 mm (approximately 12.24% of the tibial length) away from the distal end of the VOI. The μFE models were solved using ANSYS (Version 15.0, ANSYS, Inc., Cannonsburg, PA, USA) on a workstation (Intel Xeon E-5-2670, 2.60 GHz, 256 GB RAM). It took approximately 65 minutes for one FE simulation.

2.5 Statistical analysis

The effects of OVX intervention on the structural (TEA, TPA and BV), densitometric (BMC and TMD) and mechanical (stiffness and failure load) properties of mouse tibiae were analyzed using analysis of covariance (ANCOVA) (adjusted for the baseline values at week 14). The effect of ionizing radiation on these parameters was analyzed using paired t-tests by comparing the values between the irradiated and non-irradiated limbs at week 24. Linear regression equations and the coefficients of determinations (R^2) were computed to determine the relationships between tibial BMC and stiffness and between tibial BMC and failure load. Data are presented as the mean ± standard deviation (SD) unless otherwise specified. Analysis was performed in R software (https://www.r-project.org/). The probability of

type I error was set to α=0.05; i.e., *p* values < 0.05 are considered statistically significant.

3 Results

3.1. Effect of ionizing radiation on TEA, TPA, BV, TMD, BMC, stiffness and failure load

Eight *in vivo* longitudinal scans led to a decrease in TEA and increases in TPA, BV, TMD and BMC in both the OVX and SHAM groups across the whole tibia with no regional dependence (**Table 1**). The radiation-induced differences, normalized with respect to the values in the non-irradiated tibiae, were similar in both the OVX and SHAM groups, for example, -3.6 ± 1.1% (range from -5.3% to -1.6%; OVX) vs -3.4 ± 1.3% (range from -5.1% to -1.8%; SHAM) for the total TEA; 4.4 ± 0.9% (range from 3.1% to 5.8%; OVX) vs 4.8 ± 0.7% (range from 3.5% to 5.9%; SHAM) for the total BMC (all $p > 0.05$, **Table 1**).

The *in vivo* scans led to increased stiffness and failure load in both the OVX and SHAM groups, as predicted by the FE models. However, the increases in these parameters were similar between the OVX and SHAM groups, i.e., 4.6 ± 1.1% (range from 6.3% to 3.1%; OVX) vs 4.4 ± 1.3% (range from 6.1% to 2.8%; SHAM) for the stiffness; 5.6 ± 1.1% (range from 7.3% to 3.6%; OVX) vs 5.4 ± 1.2% (range from 7.1% to 3.8%; SHAM) for the failure load.

3.2. Measurement errors associated with the image processing pipeline

The precision errors for the bone parameters were almost homogenous along the tibial length (**Table 2**). To be conservative, the precision errors for regional BMC, TMD, BV, TEA and TPA were chosen to be 2.5%, 2.0%, 2.5%, 1.5% and 1.0%,

respectively, for subsequent analysis in the present study. Therefore, only differences smaller than or larger than these values can be interpreted as between-group differences. Regional BMC, BV, TEA and TPA have large ICCs (0.86 to 0.99) (**Table 2**), which means that for these parameters, the inter-subject differences are larger than the repeated-scan differences. Regional TMD has small ICCs (0.26 to 0.84) (**Table 2**); the reason for this could be that the differences in TMD between mice are small.

3.3. Effect of OVX on tibial length, TEA, TPA, BV, TMD and BMC

OVX did not have a significant influence on the tibial length from week 16 to week 22 (all $p > 0.05$, **Fig. 2**). Tibial length continuously increased from week 14 to week 22, but the magnitude of the increase was small in both groups. Using the values at week 14 as the baseline, tibial length at week 22 increased by 3.74% and 2.53% in the OVX and SHAM groups, respectively (**Fig. 2**).

OVX led to significantly increased TEA in most tibial compartments four weeks after intervention (week 18) (**Fig. 3a and 3b**, and **Fig. 4a,** most $p < 0.05$) but did not significantly alter TPA (**Fig. 3c and 3d**, and **Fig. 4b,** all $p > 0.05$). From week 14 to week 22, TEA decreased in the SHAM group (**Fig. 3a**). After OVX, the rate of TEA decreased slowed, and TEA increased in some tibial compartments (e.g., C07 to C10 compartments), e.g., at week 22 in compartment C07, with respect to the baseline (week 14) values, TEA decreased by 6% in the SHAM group and increased by 7% in the OVX group (**Fig. 3a and 3b**). From week 14 to week 22, TPA increased in most compartments in both the SHAM (**Fig. 3c**) and OVX groups, e.g., at week 22 in compartment C07, with respect to the baseline values, TPA increased by 14% and 17% in the SHAM and OVX groups, respectively (**Fig. 3c and 3d**).

Two weeks after OVX (week 17), BV and BMC significantly decreased only in the proximal compartments (C01Ct, C01 and C02) (**Fig. 4c and 4d,** all $p < 0.05$), but TMD was not significantly changed in any of the compartments (**Fig. 4e,** all $p > 0.05$). For example, at week 22 in C01 (tibial proximal region), with respect to the values in the SHAM group, OVX intervention led to a 9% decrease in BV ($p < 0.05$), a 14% decrease in BMC ($p < 0.01$) and a 4% decrease in TMD ($p > 0.05$); at week 22 in C04 (tibial midshaft), with respect to the values in the SHAM group, OVX intervention led to a 4% increase in BV, a 2% increase in BMC and a 2% decrease in TMD (all $p > 0.05$).

3.4. Effect of OVX on total tibial BMC, stiffness, failure load and correlation analysis

OVX did not have a significant influence on tibial BMC, stiffness and failure load from week 16 to week 22 (all $p > 0.05$, **Fig. 5**). The tibial BMC, stiffness and failure load continuously increased from week 14 to week 22 (**Fig. 5**). Eight weeks after OVX (week 22), the values, normalized with respect to the baseline values, in the OVX and SHAM groups were 22.01 ± 4.07% (OVX) vs 25.95 ± 4.27% (SHAM) for the total BMC, 11.54 ± 2.96% vs 12.13 ± 2.08% for the stiffness and 14.50 ± 3.25% vs 16.16 ± 2.76% for the failure load (all $p > 0.05$, **Fig. 5**).

Both the tibial stiffness and failure load were highly linearly correlated with the total BMC for both the pooled data (stiffness: $R^2 = 0.83$; failure load: $R^2 = 0.73$) and the data separated between the OVX (stiffness: $R^2 = 0.82$; failure load: $R^2 = 0.74$) and SHAM groups (stiffness: $R^2 = 0.86$; failure load: $R^2 = 0.81$) (**Fig. 6**).

Neither the OVX nor the age (from 14 to 22 weeks old) had a significant influence on the pattern of the distribution of the 1st and 3rd principal strains over the

whole mouse tibia (**Fig. 7**). All failures occurred in the compressive loading mode and in the same location of mouse tibia (**Fig. 7**).

4 Discussion

In the present study, the longitudinal effect of OVX intervention on the structural, densitometric and mechanical properties of bone across the whole mouse tibia was investigated using a novel approach combining *in vivo* μCT imaging, spatiotemporal analysis and finite element modeling.

It should be noted in the present study that the spatiotemporal analysis approach allows more precise quantification of bone changes than the standard 3D morphological analysis [27] and a comprehensive investigation of not only the regional effect but also the temporal effect (**Fig. 4**). It also should be noted that the present study is the first application of longitudinal μCT imaging in characterizing the behavior of whole bone (tibia). This is necessary for two main reasons: first, it allows analysis of the mechanical behavior of the whole tibia, e.g., the stiffness and failure properties, which are fundamental for determining whether the pre-clinically tested intervention would be effective in improving the bone competence for resisting fractures (the final clinical goal of anti-osteoporosis treatments); second, it allows correlation analysis between the local bone adaptations and the changes in global behaviors and thus could provide a comprehensive analysis of the mechanism of bone adaptation induced by osteoporosis.

The data in the present study revealed that OVX significantly led to bone loss at the endosteal surface in most compartments after five weeks of intervention but induced no significant changes on the tibial periosteal surface, which is in good agreement with the literature.[2,6] However, the present study is the first to extend the

data to the spatiotemporal space across the whole tibia. It should be noted that compared with the periosteal surface, the endosteal surface could be subjected to more fluid flows, but the relationship between fluid flow and the decrease in TEA requires further investigation. Second, the data revealed that OVX led to significant reductions in tibial BV and BMC only in the proximal regions rather than across the whole tibial region. This finding agrees with the literature data that OVX-induced differences were more pronounced at trabecular sites than at cortical sites,[6] and no significant effects induced by OVX were detected at the femur midshaft of C57BL/6J mice[2]. One reason for the decreases in BMC in the proximal regions is the loss of trabecular bone in these regions. However, for the first time, it was revealed in the present study that the cortical BV and BMC in the proximal regions (C01Ct) were also reduced. One possible explanation for the decreases only in the proximal regions is that there are many young, growing and porous bones in the proximal regions (close to the growth plate), which make the response to OVX intervention in the proximal regions much more pronounced than that in other regions (e.g., midshaft). The finding that OVX intervention has no significant effect on TMD agrees well with Easley et al.'s study, in which the bone tissue mineralization was found to have a minimal contribution to the intervention-induced bone changes.[28] Third, the data in the present study revealed that OVX led to significantly reduced BV and BMC only in the proximal regions (C01 and C02) of the tibia, and these reductions were not sufficient to significantly reduce the total tibial BMC, the stiffness and failure load predicted by the FE analysis, at least in the simulated compression scenario. This implies that the current animal model of osteoporosis may not be able to simulate the reduced bone competence for resisting fractures in osteoporotic bones. Because of the high correlations between the tibial failure load and total BMC, reduction of the

total BMC of the bone may be a future direction for developing appropriate animal models of osteoporosis.

Because *in vivo* μCT imaging is based on ionizing radiation, the damage to bone tissues caused by the radiation could affect the outcomes of this study. It was found that eight *in vivo* scans led to altered bone properties. This is in agreement with previous studies in which it was found that irradiation resulted in an increase in cortical bone density[29] and a substantial loss of trabecular bone.[30] However, the magnitudes of the radiation-induced increases in the TPA, BV, TMD, BMC, stiffness and failure load, and the decrease in TEA were similar in both the OVX and SHAM groups. Therefore, the method in the present study is valid for evaluating the OVX-induced changes.

It should be noted that, in the present study, the period of OVX is eight weeks, while this period is approximately five weeks [2,6] or up to 12 weeks in other studies.[9] In principle, a longer OVX period is better for detecting the effect of the intervention but will involve more radiation and cause more pain for the mouse. It should also be noted that the standardized method (i.e., selecting the four most proximal and distal layers for applying the boundary conditions and a region 2.06 mm away from the proximal end and 1.77 mm way from the distal end for calculating the failure load) was used in the μFE models. However, because of the small inter-sample variations and the small longitudinal increase in tibial length from 14 to 22 weeks of age, this method will result in almost the same areas for boundary conditions and the same regions of investigation for calculating the failure load.

There are several limitations related to the experimental work performed in the present study. First, rigid registration was used to align the image datasets. To eliminate the effect of skeletal growth on the results, the technique of full elastic

registration [31] should be used. However, the precision and accuracy of the elastic registration need to be investigated first to assure that the image interpolation used in the elastic registration does not induce larger errors than those obtained from the current approach. On the other hand, in the present study, the mice aged from 14 to 22 weeks old were chosen for investigation in order to minimize the effect of tibial growth on the results. Indeed, the tibial length was found to be stabilized during this period, which is in accordance with literature data.[32,33] However, the present study offers more details owing to its weekly investigation compared with the monthly interval in other studies.[32,33] Furthermore, in the present study, the rigid registration was performed in a stepwise manner, which justified the method. Second, a relatively small number of animals (N = 6) was used in this study, which may prevent the detection of significant differences between the OVX and SHAM groups. However, the mice came from the same strain and were housed and raised in the same conditions. The inter-sample differences are believed to be much smaller than the differences caused by the medical intervention. Finally, the tibia was chosen as the bone for the investigation of osteoporosis, but the tibia is not generally a bone that suffers osteoporotic fractures in humans. However, mouse bones have a very different loading mechanism compared to human bones, and even mouse femur cannot be used to properly simulate the osteoporotic fractures in humans. On the other hand, the main aim of the present study was to demonstrate the application of a novel spatiotemporal approach in the comprehensive analysis of bone adaptations in the spatiotemporal space. Once the data for other sites and species are available, the approach can be easily transferred to provide more clinically meaningful values.

With regard to the FE analysis, first, although bone is intrinsically anisotropic and heterogeneous,[34] linear elastic and subject-specific homogenous μFE models

were used to predict the stiffness and failure load of mouse tibiae in the loading scenario of uniaxial compression in the present study. The main reasons for using homogeneous instead of heterogeneous models are that the local value of bone mineral density at the image voxel level may be easily affected by image noise and is not reproducible[17] and that the density-modulus relationship for mouse tibiae at the μCT image voxel level is still unclear. The reason for using voxel meshes instead of smooth tetrahedral meshes is to avoid the modification of the actual geometry of mouse tibiae in the image smoothing process. Recent studies using bovine and human bone samples [35,36] have shown that the distribution of local displacement and the stiffness of bone can be accurately predicted using linear elastic and homogenous μFE models. To the authors' knowledge, direct validation of the μFE models for different failure criteria has not been performed so far. However, in the present study, the same failure criterion for each model (across mice, groups and age) was applied in order to compare the predicted failure load among mice. In the present study, the uniaxial compression scenario of the bone was simulated. It should be noted that in reality, the loading scenario for the osteoporotic fracture of mouse tibiae is much more complex. However, because osteoporosis is a systematic disease that increases bone weakness, the decrease in the mechanical properties of whole bone should occur not only in the fracture loading case but also in the uniaxial compression case. In addition, the uniaxial compression loading scenario is widely used in the literature and thus facilitates comparisons with other studies.[14,23,37] Additionally, other loading scenarios such as three-point bending tests are scarcely informative of the changes in bone strength induced by the changes in some local regions of the bone. For example, if the local bone adaptations lead to a failure in the midshaft (position of loading in three-point bending test) of mouse tibiae, failure load

of the tibia cannot be properly predicted by the FE models because of the removal of the region of interest close to the boundary conditions (Saint Venant's principle). It should be noted that the midshaft of mouse tibiae has the highest principal strains during locomotion,[38] and thus, this region is at high risk of fracture compared to other regions. Finally, the intra-cortical porosity was not measured in the μCT images and not incorporated into the FE model. The reason for this is that the *in vivo* μCT image resolution of 10.4 μm is not sufficient to make accurate measurements of intra-cortical porosity in mouse tibiae. However, it should be noted that the large pores within the cortex were segmented and considered in the FE models.

In summary, this study demonstrated the application of a novel spatiotemporal approach in the investigation of the longitudinal effect of OVX on bone properties. Using this approach, several additional and important findings were revealed. For example, OVX induced bone loss only at the tibial endosteal surface and not at the periosteal surface; OVX led to significantly reduced bone volume and BMC only in the proximal regions, but these reductions did not have a significant influence on the total tibial BMC, stiffness and failure load. The spatiotemporal approach can be used to conduct comprehensive analyses of the changes in bone properties in other scenarios in preclinical animal studies.

Conflict of interest statement

The authors declare that there are no financial or personal relationships with other persons or organizations that might inappropriately influence this work.

Acknowledgements

This work was funded by the National Natural Science Foundation of China (11702057, 11772086), and the Open Fund from the State Key Laboratory of Structural Analysis for Industrial Equipment (GZ1611).

The raw data analyzed and reported in this paper are obtained from the project funded by the UK National Centre for the Replacement, Refinement and Reduction of Animals in Research (NC3Rs), grant number: NC/K000780/1. The raw data are available in Open Access under CC-BY-NC license and can be retrieved with the following DOI: 10.15131/shef.data.3814701.

References

1. Riggs, B.L. and Melton, L.J. The worldwide problem of osteoporosis: insights afforded by edidemiology. *Bone* 17, 505s-511s, 1995.
2. Bouxsein, M.L., Myers, K.S., Shultz, K.L., Donahue, L.R., Rosen, C.J. and Beamer, W.G. Ovariectomy-induced bone loss varies among inbred strains of mice. *J. Bone Miner Res.* 20, 1086-1092, 2005.
3. Boyd, S.K., Davison, P., Müller, R. and Gasser, J.A., Monitoring individual morphological changes over time in ovariectomized rats by in vivo micro-computed tomography. *Bone* 39: 854-862, 2006.
4. Laib, A., Kumer, J.L., Majumdar, S. and Lane, N.E. The temporal changes of trabecular architecture in ovariectomized rats assessed by microCT. *Osteoporos Int.* 12, 936-941, 2001.
5. Laib, A., Barou, O., Vico, L., Lafage-Proust, M.H., Alexandre, C. and Rügsegger, P.. 3D micro-computed tomography of trabecular and cortical bone architecture with application to a rat model of immobilisation osteoporosis. *Med. Biol. Eng. Comput.* 38, 326 – 332, 2000.

6. Klinck, J. and Boyd, S.K. The magnitude and rate of bone loss in ovariectomized mice differs among inbred strains as determined by longitudinal in vivo micro-computed tomography. *Calcif Tissue Int.* 83: 70-79, 2008.

7. Altman, A.R., Tseng, W.J., de Bakker, C.M., Chandra, A., Lan, S., Huh, B.K., Luo, S., Leonard, M.B., Qin, L. and Liu, X.S. Quantification of skeletal growth, modeling, and remodeling by in vivo micro computed tomography. *Bone* 81: 370-379, 2015.

8. Birkhold, A.I., Razi, H., Weinkamer, R., Duda, G.N., Checa, S. and Willie, B.M.. Monitoring in vivo (re)modeling: a computational approach using 4D microCT data to quantify bone surface movements. *Bone* 75: 210-221, 2015.

9. Lambers, F.M., Kuhn, G., Schulte, F.A., Koch, K. and Müller, R. Longitudinal assessment of in vivo bone dynamics in a mouse tail model of postmenopausal osteoporosis. *Calcif. Tissue. Int.* 90: 108 -119, 2012.

10. Campbell, G.M., Tiwari, S., Grundmann, F., Purcz, N., Schem, C. and Gluer, C.C. Three-dimensional image registration improves the long-term precision of in vivo micro-computed tomographic measurements in anabolic and catabolic mouse models. *Calcif.Tissue Int.* 94: 282-292, 2014.

11. Campbell, G.M., Bernhardt, R., Scharnweber, D. and Boyd, S.K.. The bone architecture is enhanced with combined PTH and alendronate treatment compared to monotherapy while maintaining the state of surface mineralization in the OVX rat. *Bone* 49: 255-232, 2011.

12. Ausk, B.J., Huber, P., Srinivasan, S., Bain, S.D., Kwon, R.Y., McNamara, E.A., Poliachik, S.L., Sybrowsky, C.L. and Gross, T.S. Metaphyseal and diaphyseal bone loss in the tibia following transient muscle paralysis are spatiotemporally distinct resorption events. *Bone* 57(2): 413-422, 2013.

13. Levchuk, A., Zwahlen, A., Weigt, C., Lambers, FM, Badilatti, S.D., Schulte, F.A., Kuhn. G. and Mueller, R. Large scale simulations of trabecular bone adaptation to loading and treatment. *Clin Biomech* 29(4): 355-362, 2014.

14. Razi, H., Birkhold, A.I., Zaslansky, P., Weinkamer, R., Duda, G.N., Willie, B.M. and Checa, S. Skeletal maturity leads to a reduction in the strain magnitudes induced within the bone: a murine tibia study. *Acta Biomater* 13: 301-10, 2015.

15. de Bakker, C.M., Altman, A.R., Tseng, W.J., Tribble, M.B., Li, C., Chandra, A., Qin, L, and Liu XS. microCT-based, in vivo dynamic bone histomorphometry allows 3D evaluation of the early responses of bone resorption and formation to PTH and alendronate combination therapy. *Bone* 73: 198-207, 2015.

16. Pereira, A.F., Javaheri, B., Pitsillides, A.A. and Shefelbine, S.J. Predicting cortical bone adaptation to axial loading in the mouse tibia. *J R Soc Interface* 12(110):0590, 2015.

17. Lu, Y., Boudiffa, M., Dall Ara, E., Bellantuono, I. and Viceconti, M. Development of a protocol to quantify local bone adaptation over space and time: quantification of reproducibility. *J. Biomech.* 49: 2095-2099, 2016.

18. Buie, H.R. and Campbell, G.M., Klinck, J., MacNeil, J.A. and Boyd, S.K. Automatic segmentation of cortical and trabecular compartments based on a dual threshold technique for in vivo micro-CT bone analysis. *Bone* 41: 505-515, 2007.

19. Lu, Y., Boudiffa, M., Dall Ara, E., Bellantuono, I. and Viceconti, M. Evaluation of in-vivo measurement errors associated with micro-computed tomography scans by means of the bone surface distance approach. *Med. Eng. Phys.* 37: 1091-1097, 2015.

20. Bouxsein, M.L., Boyd, S.K., Christiansen, B.A., Guldberg, R.E., Jepsen, K.J. and Müller, R. Guidelines for assessment of bone microstructure in rodents using microcomputed tomography. *J. Bone Miner Res.* 25(7): 1468-1486, 2010.

21. Vickerton, P., Jarvis, J.C., Gallagher, J.A., Akhtar, R., Sutherland, H. and Jeffery, N., Morphological and histological adaptation of muscle and bone to loading induced by repetitive activation of muscle. *Proc. Biol. Sci./R. Soc.* 281: 20140786, 2014.

22. Webster, D.J., Morley, P.L. van Lethe, G.H. and Mueller, R. A novel in vivo mouse model for mechanically stimulated bone adaptation – a combined experimental and computational validation study. *Comput. Methods Biomech. Biomed. Eng*. 11, 435-441, 2008.

23. Patel, T.K., Brodt, M.D., Silva, M.J. Experimental and finite element analysis of strains induced by axial tibial compression in young-adult and old female C57Bl/6 mice. *J. Biomech*, 47: 451-457, 2014.

24. Pistoia, W., van Rietbergen, B., Lochmueller, E.M., Lill, C.A., Eckstein, F. and Ruegsegger, P. Estimation of distal radius failure load with micro-finite element analysis models based on three-dimensional peripheral quantitative computed tomography images. *Bone* 30(6): 842 -848, 2002.

25. Qasim, M., Farinella, G., Zhang, J., Li, X., Yang, L., Eastell, R. and Viceconti M. Patient-specific finite element estimated femur strength as a predictor of the risk of hip fracture: the effect of methodological determinants. *Osteoporos Int* 27(9): 2815-2822, 2016.

26. Bayraktar, H.H., Morgan, E.F., Niebur G.L.., Morris, G.E., Wong, E.K. and Keaveny, T.M. Comparison of the elastic and yield properties of human femoral trabecular and cortical bone tissue. *J Biomech* 37: 27-35, 2004.

27. Lu, Y., Boudiffa, M., Dall'Ara, E., Liu, Y., Bellantuono, I., Viceconti, M. Longitudinal effects of Parathyroid Hormone treatment on morphological, densitometric and mechanical properties of mouse tibia. *J. Mech Behav Biomed Mater*. 75: 244-251, 2017.

28. Easley, S.K., Jekir, M.G., Burghardt, A.J., Li, M. and Keavey, T.M. Contribution of the intra-specimen variations in tissue mineralization to PHT- and raloxifene-induced changes in stiffness of rat vertebrae. *Bone* 46: 1162-1169, 2010.

29. Wernle, J.D., Damron, T.A., Allen, M.J. and Mann, K.A. Local irradiation alters bone morphology and increases bone fragility in a mouse model. *J. Biomech*. 43: 2738-2746, 2010.

30. Klinck, J., Campbell, G.M. and Boyd, S.K. Radiation effects on bone architecture in mice and rats resulting from in vivo micro-computed tomography scanning. *Med Eng Phys.* 30, 888-895, 2008.

31. Dall'Ara, E., Barber, D. and Viceconti, M. About the inevitable compromise between spatial resolution and accuracy of strain measurement for bone tissue: a 3D zero-strain study. *J Biomech.* 47: 2956-2963, 2014.

32. Glatt, V., Canalis, E., Stadmeyer, L. and Bouxsein, M.. Age-related changes in trabecular architecture differ in female and male C57BL/6J mice. *J Bone Miner Res*. 22(8): 1197-1207, 2007.

33. Somerville, J.M., Aspden, R.M., Armour, K.E. and Reid, D.M. Growth of C57Bl/6 mice and the material and mechanical properties of cortical bone from the tibia. *Calcif Tisse Int.* 74: 469-475, 2004.

34. Ashman, R.B., Cowin, S.C., van Bushirk, W.C. and Rice, J.C. A continuous was technique for the measurement of the elastic properties of cortical bone. *J. Biomech* 19: 349-361, 1984.

35. Chen, Y., Dall'Ara, E., Manda, K., Sales, E., Wallace, R. and Pankaj, P. Micro-CT based finite element models of cancellous bone predict accurately displacement once the boundary condition is well replicated: a validation study. *J Mech Behav Biomed Mater*. 65: 644-651, 2017.

36. Costa, M.C., Tozzi, G., Cristofolini, L., Danesi, V., Viceconti, M. and Dall'Ara, E. Micro finite element models of the vertebral body: validation of local displacement predictions. *PLoS One*, 12(7): e0180151, 2017.

37. Yang, H., Butz, K.D., Duffy, D., Niebur, G.L., Nauman, E.A. and Main, R.P. Characterization of cancellous and cortical bone strain in the in vivo mouse tibial loading model using microCT-based finite element analysis. *Bone* 66: 131-9, 2014.

38. Prasad, J., Wiater, B.P., Nork, S.E., Bain, S.D. and Gross, T.S. Characterizing gait induced normal strains in a murine tibia cortical bone defect model. *J. Biomech*, 43: 2765-2770, 2010.

Table 1. Relative differences between the irradiated and non-irradiated tibiae in terms of the structural (TEA, TPA and BV) and densitometric (TMD and BMC) properties of mouse tibiae in the OVX and SHAM groups across the whole tibia (N = 6 per group). Data are presented as the radiation-induced differences normalized with respect to the values in the non-irradiated tibiae at 24 weeks of age.

	TEA		**TPA**		**BV**		**TMD**		**BMC**	
	SHAM	OVX	SHAM	OVX	SHAM	OVX	SHAM	OVX	SHAM	OVX
C01	-3.2 ± 2.5%	-4.8 ± 1.6%	4.2 ± 1.4%	3.9 ± 2.3%	5.8 ± 2.7%	4.8 ± 1.4%	1.8 ± 2.1%	1.6 ± 1.1%	4.5 ± 1.3%	4.3 ± 1.6%
C02	-4.8 ± 2.2%	-3.4 ± 1.3%	4.4 ± 1.6%	2.4 ± 1.5%	5.6 ± 1.8%	4.6 ± 2.2%	2.4 ± 1.0%	2.6 ± 1.2%	3.3 ± 1.4%	4.6 ± 2.2%
C03	-2.4 ± 1.6%	-4.8 ± 1.9%	2.8 ± 1.6%	2.2 ± 1.5%	5.4 ± 1.6%	5.2 ± 1.5%	2.2 ± 1.2%	2.5 ± 1.3%	5.5 ± 2.1%	4.5 ± 1.6%
C04	-4.9 ± 2.9%	-2.5 ± 2.7%	4.8 ± 1.7%	3.8 ± 1.7%	4.2 ± 1.6%	5.2 ± 2.3%	2.6 ± 1.6%	2.4 ± 1.6%	6.1 ± 2.3%	5.4 ± 1.6%
C05	-5.0 ± 2.1%	-3.0 ± 2.5%	2.9 ± 1.5%	3.5 ± 1.4%	4.8 ± 1.5%	5.8 ± 2.4%	2.5 ± 1.4%	1.5 ± 1.3%	5.9 ± 2.2%	5.5 ± 1.4%
C06	-2.3 ± 1.5%	-5.3 ± 2.2%	3.3 ± 1.2%	3.3 ± 3.7%	5.9 ± 2.3%	4.9 ± 1.3%	2.9 ± 1.5%	1.9 ± 1.4%	4.7 ± 1.7%	4.9 ± 1.8%
C07	-5.1 ± 2.0%	-4.6 ± 1.7%	5.6 ± 1.3%	4.6 ± 1.5%	4.1 ± 1.1%	4.4 ± 1.2%	2.2 ± 1.1%	1.2 ± 0.9%	4.6 ± 1.8%	4.2 ± 1.3%
C08	-3.4 ± 1.9%	-4.4 ± 2.8%	3.4 ± 1.3%	4.4 ± 1.8%	4.5 ± 1.4%	4.1 ± 2.4%	2.0 ± 0.9%	1.6 ± 1.0%	3.4 ± 2.2%	3.6 ± 2.0%
C09	-4.0 ± 2.1%	-5.3 ± 1.6%	5.0 ± 1.5%	5.8 ± 1.9%	5.5 ± 1.7%	5.8 ± 2.7%	1.9 ± 1.4%	1.9 ± 1.1%	4.8 ± 1.5%	4.4 ± 1.5%
C10	-4.6 ± 1.9%	-3.4 ± 1.8%	4.4 ± 1.6%	4.7 ± 2.4%	5.7 ± 1.8%	5.5 ± 1.5%	2.5 ± 1.7%	2.4 ± 1.3%	3.4 ± 1.8%	3.6 ± 1.6%
Whole tibia	-3.4 ± 1.3%	-3.6 ± 1.1%	3.3 ± 1.1%	3.4 ± 1.2%	4.7 ± 0.8%	4.5 ± 0.9%	2.3 ± 0.9%	2.2 ± 0.8%	4.8 ± 0.7%	4.4 ± 0.9%

Table 2. Reproducibility of BV, TMD, BMC, TEA and TPA expressed as mean precision errors (PEs) as coefficients of variation (the 95% confidence intervals are shown in square brackets) and intraclass correlation coefficients (ICC) (8 mice and 4 scans per mouse) (C01 – C10 correspond to tibial proximal to distal sides; see Figure 1f).

	BV		**TMD**		**BMC**		**TEA**		**TPA**	
	PE [%]	ICC	PE[%]	ICC	PE[%]	ICC	PE[%]	ICC	PE[%]	ICC
C01	1.98 [1.6 2.6]	0.94	1.41 [1.1 1.9]	0.84	2.01 [1.7 2.5]	0.96	0.93 [0.8 1.2]	0.97	0.73 [0.6 0.9]	0.98
C02	1.66 [1.3 2.2]	0.95	1.34 [1.1 1.8]	0.70	1.64 [1.4 2.3]	0.96	0.87 [0.7 1.1]	0.97	0.60 [0.5 0.8]	0.99
C03	1.69 [1.4 2.2]	0.94	1.43 [1.2 1.9]	0.54	1.53 [1.3 2.2]	0.95	1.03 [0.9 1.4]	0.97	0.67 [0.5 0.9]	0.98
C04	1.53 [1.2 2.0]	0.90	1.35 [1.1 1.8]	0.64	1.45 [1.2 2.0]	0.94	1.28 [1.0 1.6]	0.96	0.61 [0.5 0.8]	0.97
C05	1.29 [1.1 1.7]	0.94	1.17 [1.0 1.5]	0.56	1.47 [1.2 2.0]	0.94	0.67 [0.5 1.0]	0.99	0.58 [0.5 0.8]	0.98
C06	1.20 [1.0 1.6]	0.93	1.05 [0.9 1.4]	0.50	1.35 [1.1 1.9]	0.94	0.72 [0.6 1.0]	0.99	0.52 [0.4 0.7]	0.97
C07	1.23 [1.0 1.6]	0.92	1.15 [0.9 1.5]	0.36	1.25 [1.0 1.8]	0.93	0.87 [0.7 1.1]	0.99	0.54 [0.4 0.7]	0.98
C08	1.19 [1.0 1.6]	0.95	1.35 [1.1 1.8]	0.26	1.95 [1.6 2.4]	0.90	1.01 [0.8 1.2]	0.99	0.73 [0.6 1.0]	0.94
C09	1.24 [1.0 1.6]	0.94	1.52 [1.2 2.0]	0.26	1.72 [1.4 2.1]	0.92	1.07 [0.9 1.3]	0.99	0.46 [0.4 0.6]	0.98
C10	1.94 [1.6 2.6]	0.86	1.11 [0.9 1.5]	0.52	1.91 [1.6 2.5]	0.90	1.19 [0.9 1.4]	0.99	0.88 [0.7 1.2]	0.97

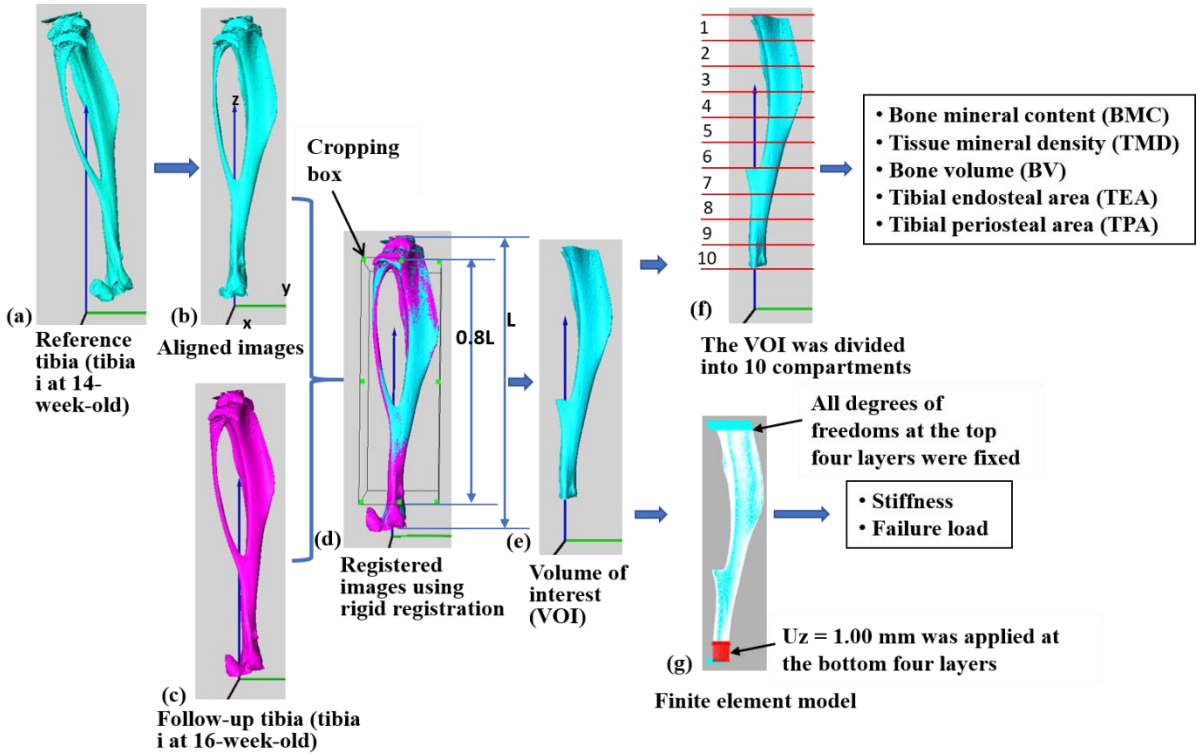

Figure 1. Schematic representation of the quantification of tibial parameters in the spatiotemporal space. (a) The baseline/reference data (one tibia from a 14-week-old mouse); (b) the aligned baseline data; (c) the follow-up data of the same tibia (tibia from the same mouse but at 16 weeks of age); (d) the registered tibial data using rigid registration; (e) the volume of interest (VOI) for investigation; (f) the spatial partition of tibial VOI and the quantification of tibial structural and densitometric parameters and (g) the setup of finite element models for the quantification of tibial mechanical parameters.

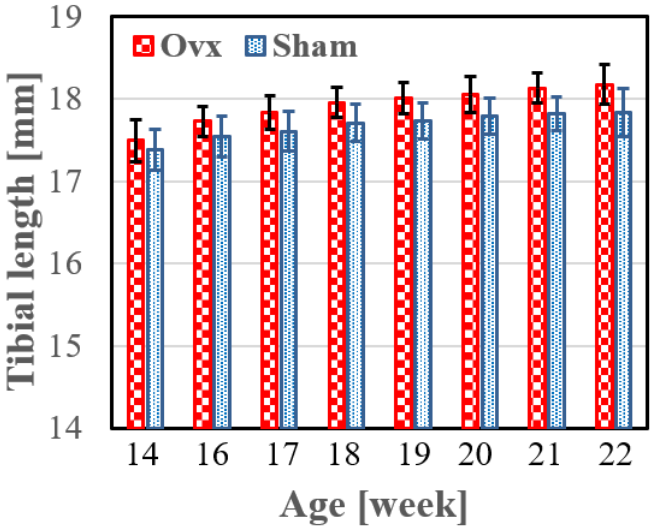

Figure 2. The longitudinal adaptations of tibial length in both the OVX and SHAM groups. Data are presented as the mean ± standard deviation of tibial length in the OVX and SHAM groups (N = 6 per group).

Normalised TEA in the SHAM group

Age [week]	16	17	18	19	20	21	22
C01	-1	-1	-2	-6	-5	-4	-3
C02	-4	-6	-7	-10	-11	-11	-9
C03	-3	-5	-6	-10	-12	-12	-11
C04	-3	-6	-7	-11	-12	-12	-11
C05	-1	-3	-4	-6	-8	-9	-7
C06	1	0	-1	-4	-7	-8	-6
C07	0	-1	-2	-5	-9	-9	-6
C08	0	-1	-2	-5	-8	-8	-4
C09	-2	-3	-2	-4	-7	-8	-8
C10	0	-1	0	-2	-3	-4	-4

(a) -20 -10 0 10 20

Normalised TEA in the OVX group

Age [week]	16	17	18	19	20	21	22
C01	7	6	4	3	1	3	4
C02	-2	-5	-1	-1	-1	0	0
C03	-1	-3	-1	-3	-4	-4	-3
C04	0	-2	-2	-5	-5	-6	-5
C05	1	-1	-1	-4	-6	-6	-5
C06	1	1	4	2	-1	-1	0
C07	3	3	6	5	4	5	7
C08	2	5	8	6	4	7	12
C09	0	5	5	4	2	2	3
C10	2	4	8	8	8	6	7

(b) -20 -10 0 10 20

Normalised TPA in the SHAM group

Age [week]	16	17	18	19	20	21	22
C01	1	3	3	3	3	5	4
C02	-1	-1	-1	-1	-1	0	0
C03	-1	0	0	0	0	1	1
C04	0	0	1	1	3	4	4
C05	1	2	3	4	6	9	10
C06	1	2	4	5	8	11	13
C07	2	3	4	6	10	13	14
C08	2	3	4	6	8	11	13
C09	1	1	2	2	3	5	5
C10	1	1	2	3	5	7	7

(c) -20 -10 0 10 20

Normalised TPA in the OVX group

Age [week]	16	17	18	19	20	21	22
C01	3	2	2	3	2	3	3
C02	3	2	5	6	5	6	4
C03	2	1	4	4	4	5	5
C04	3	2	5	5	6	6	7
C05	4	3	7	7	9	10	12
C06	4	4	8	9	11	13	15
C07	3	5	8	10	13	15	17
C08	3	5	8	10	12	15	16
C09	2	3	4	5	6	7	8
C10	3	2	5	6	8	8	9

(d) -20 -10 0 10 20

Figure 3. The longitudinal adaptations of the endosteal and periosteal areas (TEA and TPA) of mouse tibiae in the spatiotemporal space in both the OVX and SHAM groups. Data (units in percentages) are presented as the mean changes normalized with respect to the baseline values at week 14 (C01 to C10 represent compartment 01 to compartment 10 in **Fig. 1f**).

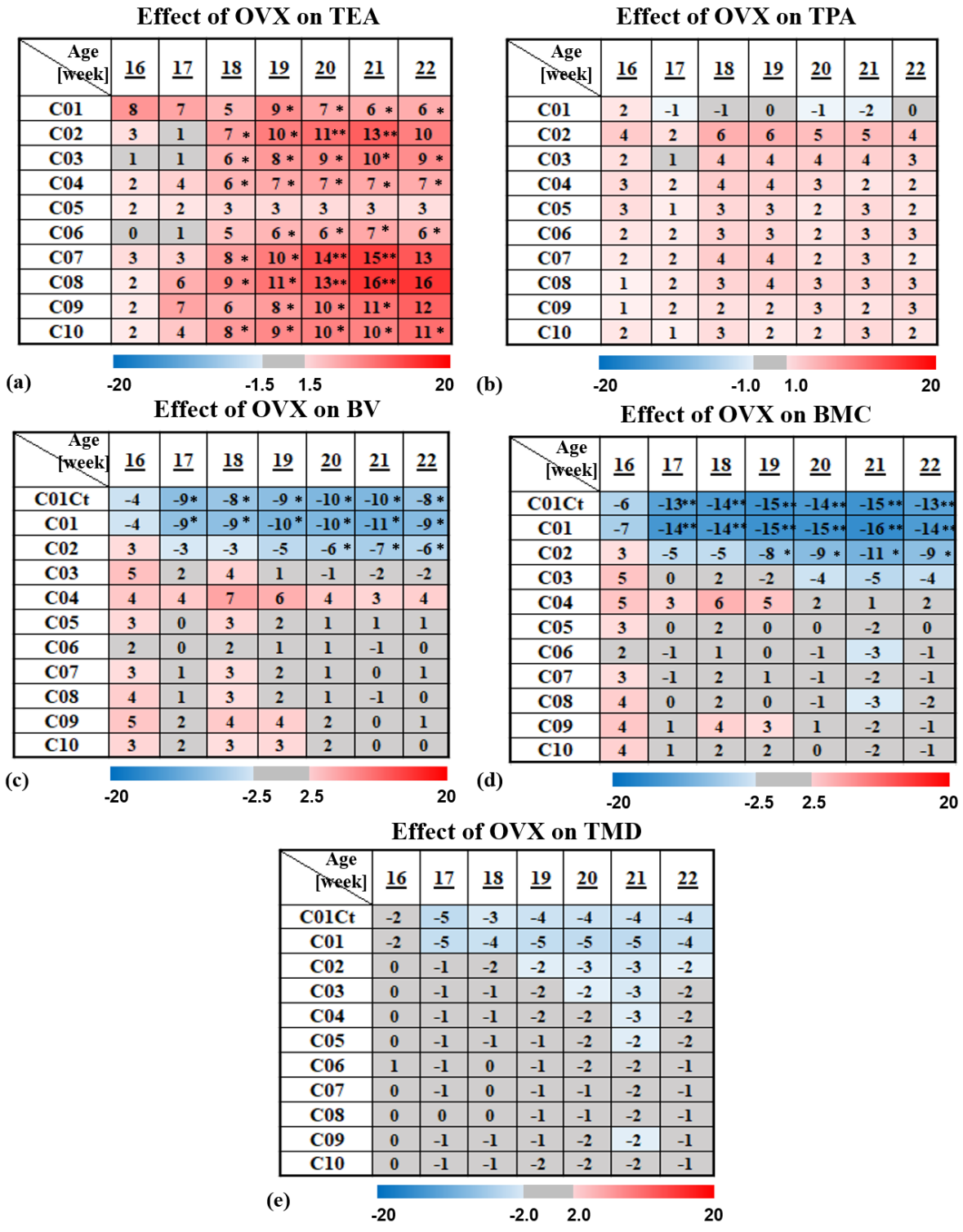

Figure 4. Longitudinal effect of OVX intervention on the structural (TEA, TPA and BV) and densitometric (TMD and BMC) properties of mouse tibiae in the spatiotemporal space. Data are presented as the mean relative percentage difference between the OVX and SHAM groups (**Equation 1**) for the 10 compartments along the tibial

proximal-distal axis (* $p < 0.05$, ** $p < 0.01$) (The cortical and trabecular parts were separated in C01, and C01Ct represents the cortical part in C01). Table color code: the gray areas are values within the ranges of measurement error; the red and blue areas represent an anabolic and a catabolic effect, respectively.

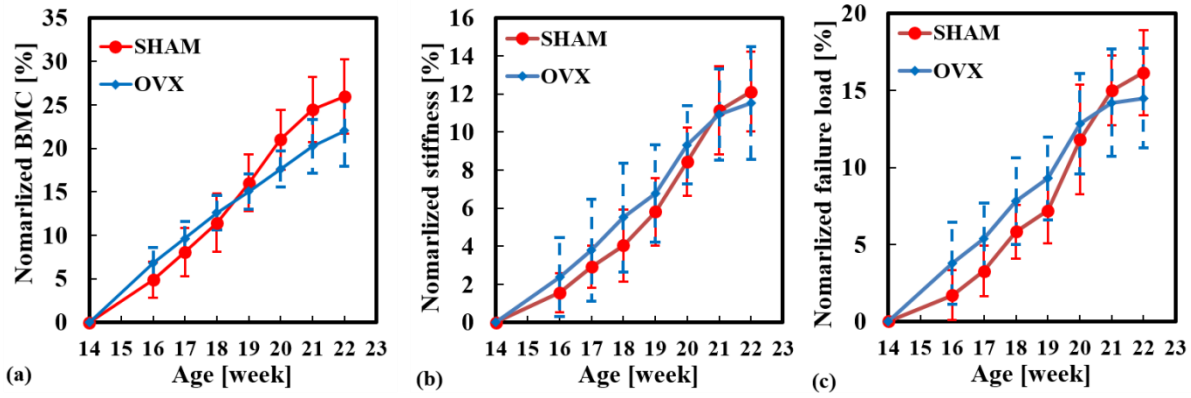

Figure 5. Longitudinal effect of OVX intervention on the total BMC, the FE predicted stiffness and failure load of mouse tibia. Data are presented as the mean ± standard deviation of the values, normalized with respect to baseline.

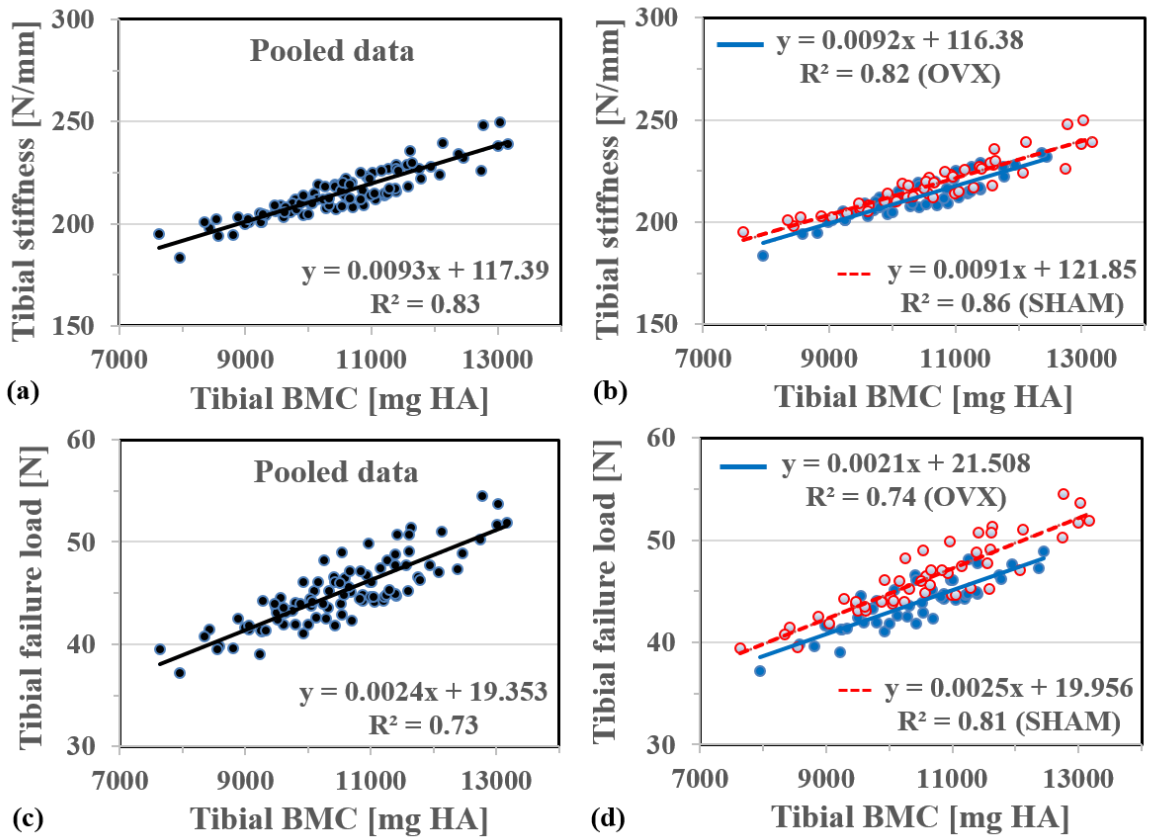

Figure 6. Linear regression analysis for FE predicted stiffness vs BMC and failure load vs BMC. (a) and (c): Analysis for the pooled data for both the OVX and SHAM groups; (b) and (d) analysis for the OVX and SHAM groups, respectively (N = 6 per group).

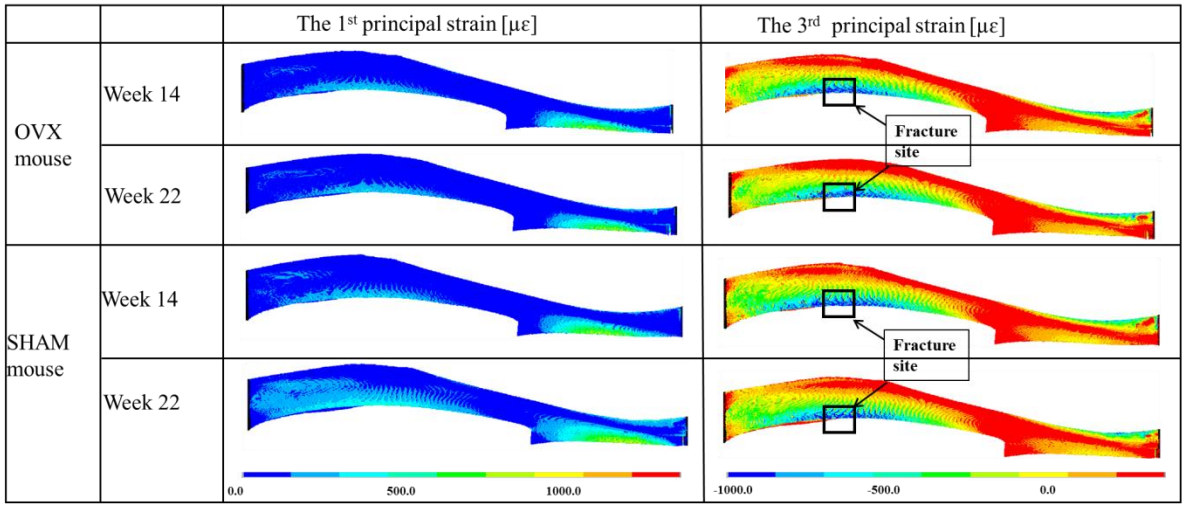

Figure 7. Distribution of the 1st and 3rd principal strains over mouse tibiae. All the images of mouse tibiae were plotted with the same view angle. The images for weeks 14 and 22 came from the same mouse in the OVX and SHAM groups.